Corrosion Fatigue Characteristics in the Weld of Multi-Pass Welded A106 Gr B Steel Pipe

Dongho Bae*
School of Mechanical Engineering, Sungkyunkwan University, Suwon, Kyonggi-do 440-746, Korea
Chul Han Kim
KNR System. Inc., Hwasung, Kyonggi-do 445-973, Korea

In order to investigate the corrosion fatigue characteristics in the weld of multi-pass welded A106 Gr B steel pipe, corrosion fatigue tests were performed under the various stress ratios and 3.5 wt% NaCl solution at room temperature. The corrosion fatigue characteristic curves were represented using crack closure concept. The obtained results are as follows; when the load frequency is 1.0 Hz, the crack opening point is transited in the region of K_{max}=20~32 MPa·$m^{1/2}$. In the low stress intensity factor range, the crack opening point is higher than that in air. However, in the high stress intensity factor range, it is lower than that in air. In the cases of 0.1 Hz and 0.01 Hz, the crack opening point gradually decreases to K_{min} with K_{max} increase.

Key Words: Corrosion Fatigue, Multi-pass Weld, Crack Closer Concept, Crack Opening Point, Stress Intensity Factor, Electro-chemical Corrosion Characteristics, Corrosion Rate

1. Introduction

Welding is practically used in every industry and is associated with a very large part of the country's gross national product. Welding processes are vital in the production and maintenance of pipelines and power plants, and in the areas of heavy construction. In many key-manufacturing operations, the vital matter of productivity is directly tied to welding.

By the way, welding processes produce residual stresses and change the metal structure as a result of the large nonlinear thermal loading created by a moving heat source. Moreover, multi-pass welding of thick section subjects the components to multiple thermal cycles and inelastic strain patterns, creating a more severe and complex residual stress distribution through the pipe thickness. And, these formidable residual stress generation and metallurgical change by the fusion welding process increase the cracking driving force and reduce the resistance of brittle fracture as well as environmental fracture (Achilles and Bulloch, 1987; ASTM Metals Hand Book, 1981; Jones, 1992; Bae et al., 2002). In particular, A106 Gr B steel, which is used in the nuclear power plant and heavy chemical plant, has been damaged during the service by various corrosion mechanisms such as corrosion fatigue. Therefore, investigating its electro-chemical corrosion mechanism and failure mechanism by the corrosion fatigue, and evaluating the fracture characteristics on the welds of the material are very important for the safety and integrity diagnoses of facilities, life prediction of the degraded materials, and establishment of the economical inspecting term. (Lim and Kim, 1997; Chung et al., 1989).

* Corresponding Author,
E-mail: dhbae@skku.edu
TEL: +82-31-290-7443; **FAX**: +82-31-295-1937
School of Mechanical Engineering, Sungkyunkwan University, Suwon, Kyonggi-do 440-746, Korea.
(Manuscript **Received** March 11, 2003; **Revised** June 25, 2003)

Thus, in this study, the electro-chemical corrosion characteristics of A106 Gr B steel were first evaluated in 3.5 wt% NaCl solution at room temperature. And next, the corrosion fatigue characteristics on the weld of multi-pass welded A106 Gr B steel pipe were investigated in the same condition. The corrosion fatigue characteristic curves according to the loading frequency were systematically evaluated using the crack closure concept.

2. Evaluation of the Electro-Chemical Corrosion Characteristics

2.1 Specimen and procedure

A twenty four-pass welded A106 Gr B steel pipe was tested in this study. Its chemical compositions, mechanical properties and welding conditions and processes are listed in Tables 1, 2 and 3, respectively. Figure 1 shows the location of the specimen in the welded pipe. The first pass was welded by GTAW (gas tungsten arc welding) and the other passes were by FCAW (flux cored arc welding). The thickness of the pipe is 30 mm and the outer diameter is 254 mm. The groove for welding was machined in a compound bevel type.

Table 1 Chemical composition of A106 Gr B steel

C	M	Si	P	S	Ni	Cr+Mo	Ni+Cu
0.01	0.86	0.21	0.01	0.004	0.10	0.06	0.39

Table 2 Mechanical properties of A106 Gr B steel

Yield strength	Tensile strength
367 MPa	486 MPa

Table 3 Welding conditions and process

	GTAW+FCAW	
	GTAW	FCAW
Gas (99.99%)	Ar	Ar
flow rate (l/min)	15~20	15~20
Filler metal	ER70S-G	E7016
Current (A)	100~120	190~210
Volts Range (V)	12~13	30~32
Travel speed (cm/min)	8~10	25~30

After cutting out a small cube of $10\times10\times10$ mm^3 from the weld metal, heat affect zone and base metal, respectively, they were mounted with epoxy resin and polished the surface of the specimen with 600-grit SiC paper.

All potentio-dynamic polarization test procedure followed the method recommended by ASTM G5 (ASTM G5, 1987) using the Potentiostat 273A (EG & G Co.). The corrosion potential was measured by using two carbon electrodes as a working electrode and a counter electrode, and one calomel electrode was used as a reference electrode.

In the beginning of the test procedure, the specimen was submerged into corrosion cell for 15 minutes in open-circuit potential status to reduce the error due to the surface conditions of the specimen. At this time, the scanning rate was 0.166 mV/sec, the range of scanning rates was $-800\sim-200$ mV, which was determined from the preliminary tests. Corrosion environment was made in 3.5 wt% NaCl solution at room temperature.

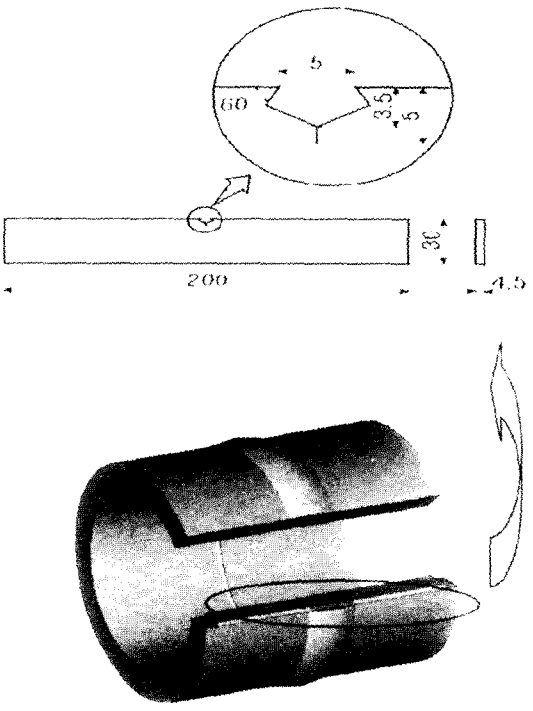

Fig. 1 Configuration and position of specimen

2.2 Electro-chemical test results and discussion

From the potentio-dynamic polarization test results on the weld of A106 Gr B steel in 3.5 wt% NaCl solution of room temperature, it was observed that the corrosion potential increased in order of the weld metal, heat affected zone and base metal. And according to the increase of corrosion potential, the increase of corrosion current density in the anode reaction was more remarkable than in cathode reaction. It indicates that the corrosion mechanism of A106 Gr B steel in NaCl solution is influenced by typical anode reaction determining the corrosion rate. This result is due to the influence of the Cl^- ion in NaCl solution that is a corrosion active factor.

In general, the Cl^- ion can easily reach and be absorbed into the metal surface under the oxide film. Being absorbed into the metal surface, it acts on a corrosion active factor and promotes degradation of the material by corrosion. These corrosion reactions concentrically reveal in the region where the protective film of passive state is relatively thin or the structure is not fine like the welds. Therefore, since the weld of A106 Gr B steel is not able to make the stable protective film on its surface, it is sensitive to corrosion than the base metal, and the degree of damage is also more severe. In order to prevent such damages, it might be necessary to secure information on the electrochemical corrosion characteristics and to develop the on-line monitoring system on the weld of the pipe in service.

Corrosion current density (i_{corr}) in the weld of A106 Gr B steel pipe can be determined using the Tafel extrapolation method from the potentio-dynamic polarization curves, and the corrosion rate is also calculated by Equation (1) recommended in ASTM G5.

$$\text{Corrosion rate (mpy)} = \frac{0.13 \times i_{corr}(\mu A/cm^2) \times E.W.}{\rho(g/cm^2)} \quad (1)$$

where i_{corr}: corrosion current density (g/cm^2), ρ: density (g/cm^2), E.W.: equivalent weight ($\sum = f_i M_i / n_i$, f_i: fraction of atom, M_i: atomic weight, n_i: atomic value). Table 4 illustrates the corrosion current density and corrosion rate calculated by the Tafel extrapolation method.

Table 4 Corrosion rate of A106 Gr B steel pipe weldment

	Base metal	HAZ	Weld metal
Corrosion rate (mm/year)	1.443×10^{-8}	4.745×10^{-8}	2.467×10^{-8}

3. Evaluation of the Corrosion Fatigue Characteristics for the Weld of A106 GR B Steel Pipe

3.1 Specimen

he material used for evaluation of the corrosion fatigue characteristics for the weld of A106 Gr B steel pipe is same with the electro-chemical tests. Configuration of the specimen is a SEN (single edge notched) type as shown in Fig. 1. An artificial notch inserted in the root of the weld where high tensile residual stress was created in the welding processes. Since the asperity and oily particles on the pipe surface affect corrosion reaction of the metal, each specimen was cleaned with the ultrasonic washer after polishing its surface. The surface of specimen except the vicinity of crack was protected from corrosive environment.

3.2 Test procedure

The fatigue tester used in this study is a hydraulic universal fatigue tester (MTS 810, capacity ; 100 kN). Loading type is a sine wave with constant amplitude of the road ratio (R) =0.1.

The maximum test load is 7840 N (800 Kgf). This value is equivalent to 15.8% of the yielding strength of the base material. Since corrosion fatigue crack growth behavior at the crack tip is influenced by holding time when the crack is fully opened, the corrosion fatigue tests were conducted in the various frequencies of 25 Hz in air and 1.0, 0.1, 0.01 Hz in 3.5 wt% NaCl solution and estimated their influence on the crack growth characteristics. Crack opening point was measured using a COD gage (gage length : 2 mm) as illustrated in Fig. 2. A corrosion cell was

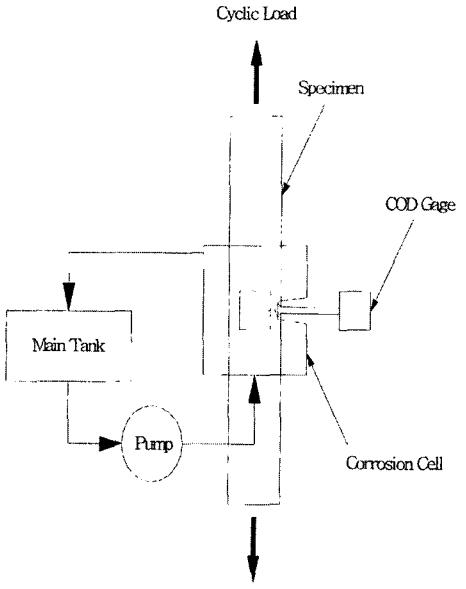

Fig. 2 Schematic of corrosion fatigue test system

specially developed for corrosion fatigue test of the SEN type specimen. It was made of acryl to prevent corrosion reaction with solution and so as to observe the surface conditions of the specimen through the attached glass. As a sealant, 3 mm thick silicone plate was used. By using 8 mm diameter spring between the specimen and cells, they could be uniformly maintained during the test. An extra waterspout was also installed to prevent the fatigue tester from corrosive and electric damage due to the solution leak. The total inner volume of the cell attached on both sides of the specimen was 10 cm^3, and the corrosive solution was circulated at the flow rate of 50 ml/min.

4. Results and Discussion

4.1 Crack growth characteristics

As loading frequency (Hz) is slow down, exposing time of the crack tip to corrosive environment becomes longer and the crack growth rate generally increases. Fig. 3 shows the relationships between the stress intensity factor range (ΔK) and crack growth rate (da/dN) in the various test conditions. The trends of the characteristic curves are similar to the results of Speidel and Vosikovsky (ASM HANDBOOK, 1996). As

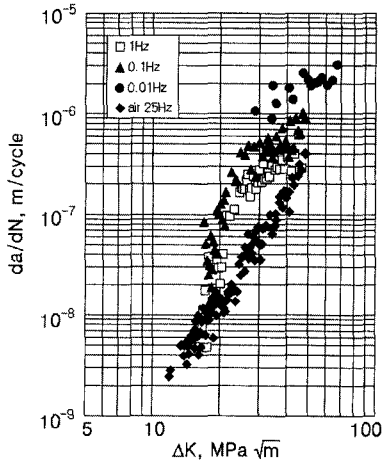

Fig. 3 Corrosion fatigue characteristic curves

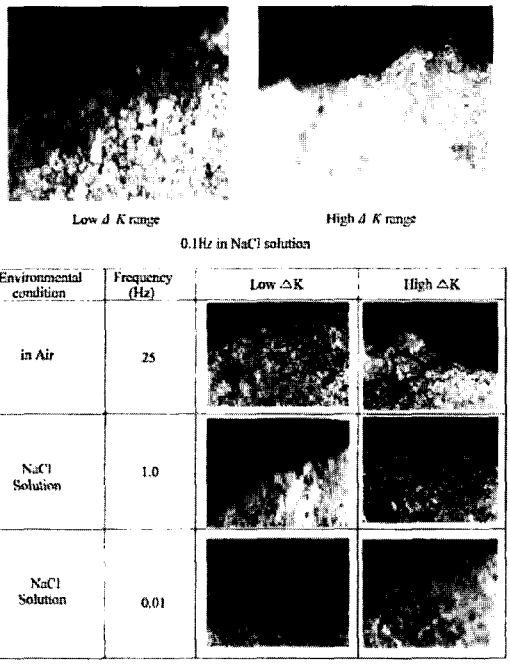

Fig. 4 Crack growth pattern in various test condition

shown in Fig. 3, in the low ΔK region ($\Delta K <$ 19 MPa·$m^{1/2}$), it is difficult to find corrosion effects on the crack growth rate. However, in the high ΔK region ($\Delta K >$ 19 MPa·$m^{1/2}$), corrosion effects are remarkable. Thus, for analyzing mechanism of the corrosion fatigue crack growth behavior according to frequency variation and for evaluating corrosion effects on the crack growth

behavior, the side views of fractured specimen was microscopically observed as shown in Fig. 4.

The crack growth pattern of specimen tested in air (Fig. 4(a)) showed transgranular in the low $\triangle K$ region, but in the high $\triangle K$ region, crack growth pattern was changed to mixed type of transgranular and intergranular. On the other hand, in case of corrosion fatigue, the intergranular pattern was observed in the low $\triangle K$ region. However, it was not clear whether this pattern was maintained during the test or not because Fig. 4 was taken after the test. Many cavities around the crack surface indicated that anodic dissolution was active during the test.

Corrosion products affect to the crack growth behavior in the various ways. First, it makes crack opening point increase due to the oxide induced by crack closure mechanism, thus the crack growth rate decreases due to actual $\triangle K_{eff}$ decrease. Second, it conversely accelerates the crack growth rate due to the wedge effect. Therefore, for reasonable evaluation of fatigue crack growth characteristics in corrosive environment, it is necessary to represent the crack growth characteristic curves shown in Fig. 3 using the effective stress intensity factor range ($\triangle K_{eff}$).

4.2 Crack closure behavior

Crack closure behaviors were summarized in Figs. 5-7. Fig. 5 shows the variation of the stress intensity factor (K_{op}) according to K_{max} increase during the test. The variation of K_{op}/K_{max} and crack opening ratio ($U=(K_{max}-K_{op})/(K_{max}-K_{min})$) are shown in Figs. 6 and 7, respectively.

4.2.1 Crack closure behavior in air

In Figures 5-7, crack closure behavior in air shows typical tendency and K_{op} is proportional to K_{max}. However, K_{op}/K_{max} is independent of K_{max}. These trends can be explained by plasticity induced crack closure mechanism. That is, plastic deformation at the crack tip generally affects crack closure.

Since the plastic deformation increases with K_{max} increase, K_{op} linearly increases with crack growth under constant amplitude loading condition.

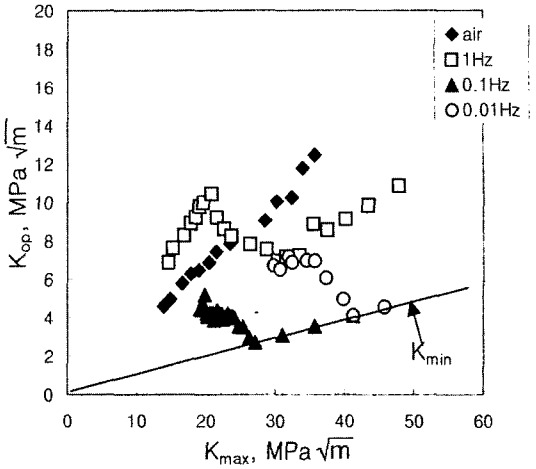

Fig. 5 Relationship between K_{op} and K_{max}

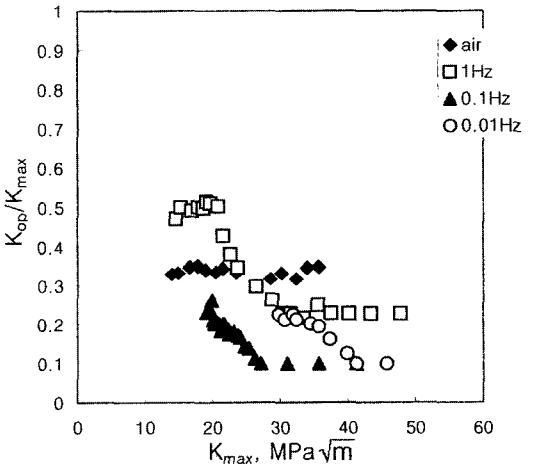

Fig. 6 Relationship between K_{op}/K_{max} and K_{max}

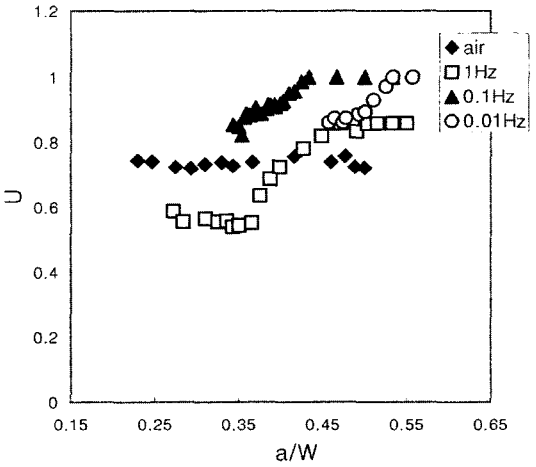

Fig. 7 Relationship between U and a/W

4.2.2 Crack closure behavior in 3.5 wt% NaCl solution

Crack closure behavior in 3.5 wt% NaCl solution shows the various trends with frequency variation. As shown in Figs. 5-7, crack closure behavior can be explained by dividing it into the three regions. In the first region where K_{max} is less than 20 MPa·$m^{1/2}$, crack closure behavior shows similar tendency with that in air, and the magnitude of K_{op} value (Fig. 5) is higher than in air. However, the crack opening ratio (U) (Fig. 6) is lower than in air. In the second region where K_{max} is 20~32 MPa·$m^{1/2}$, K_{op} decreases with K_{max} increase and the crack opening ratio shows a constant value. In the third region where Kop is more than 32 MPa·$m^{1/2}$, a similar trend to the first region is shown, but the value is lower than that in air.

These peculiar transition behaviors in crack closure phenomena can be explained by plasticity induced crack closure mechanism mentioned in 4.2.1. In corrosive environment, however, there are many factors affecting crack closure behavior such as test load, welding residual stresses, corrosion products, crack tip blunting by anodic dissolution, crack tip branching, hydrogen embrittlement, etc. Among these factors, some make crack opening point increase, and the others conversely control it. For example, when the thickness of corrosion products on the crack surface becomes larger than the crack tip opening displacement at K_{min}, crack closure behavior becomes higher. Although K_{max} is same, the thickness of corrosion products depends on the stress ratio and loading frequency. Since Hydrogen in the solution makes the plastic region of the crack tip embrittle, the crack opening point is dropped.

Welding residual stress also becomes an important factor. From the results of Shi's study (Shi et al., 1990), tensile residual stresses increase the crack opening point, and compressive residual stresses drop it. However, these effects decrease with crack growth. In the case of multi-pass welded A106 Gr B steel pipe, even though welding residual stresses around the crack tip were compressive, there was no significant effect of residual stress on the crack closer behaviors as shown in Figs. 5-7. This result can be explained by Murakami's study (Murakami et al., 1987). He studied corrosion fatigue crack growth of the weld in sea water and reported that the influence of compressive residual stress on crack growth in corrosive environment was less than that in air.

As mentioned above, in the first region of 1 Hz, crack opening point is higher than that in air. This means that corrosion products play an important role on crack closure behavior in spite of hydrogen embrittlement and relaxation of compressive residual stress. In the second region, the crack opening point decreases continuously to 7 MPa·$m^{1/2}$ and this value becomes smaller than that in air. From these results, it can be found that the influence of the crack tip opening displacement and hydrogen embrittlement on the crack closure behavior is larger than that of corrosion products. In the third region, it can be estimated that plastic deformation induced by crack closure mechanism is dominant.

Since the value of K_{op} is smaller than that in air, crack closure behavior has been affected by hydrogen embrittlement and anodic dissolution. However, it is predicted that the effect of corrosion products is very small because the increasing rate of the crack tip opening displacement becomes relatively larger than growing of the thickness of corrosion products. From the results mentioned above, it can be found that the transition behavior of crack closure is determined by reciprocal action between corrosion product and the crack tip opening displacement.

In the case of 0.1 Hz, the crack opening point decreases continuously, as shown in Figs. 5-7. When K_{max} is 27 MPa·$m^{1/2}$, K_{op} is equal to K_{max}. This means that there are no more crack closure phenomena and these results are related to the period exposed to corrosive environment. That is, the influence of electro-chemical corrosion reaction during 1 cycle increases with the loading frequency decrease. Therefore, elastic recovery around the crack tip becomes small by hydrogen embrittlement and anodic dissolution. In case of 0.01 Hz, the results similar to those of 0.1 Hz are shown qualitatively. However, the transition point is different from that of 0.1 Hz.

4.3 Representation of the crack growth characteristic curves

Many researchers showed that the fatigue crack growth characteristic curves could be represented by $\triangle K_{eff}$ in regardless of the stress ratio (Todd et al., 1997). From their results, using the crack closure concept, fatigue crack growth characteristics in the welding residual stress field can be also effectively estimated, and $\triangle K_{eff}$ in the residual stress field is given by

$$\begin{aligned}\triangle K_{eff} &= (K_{max}+K_{res})-(K_{op}+K_{res}) \\ &= K_{max}-K_{op}\end{aligned} \quad (2)$$

Since the crack closure behavior is affected by anodic dissolution and hydrogen embrittlement, the crack closure concept is useful in representation of the corrosion fatigue characteristic curves. Fig. 8 shows the corrosion fatigue characteristic curves including the crack closure concept. The bold line indicates the fatigue crack characteristic line neglecting the crack closure concept. When the crack closure concept is reflected, as shown in Fig. 8, experimental data in air are shifted in parallel to the left side in log-log scale because the magnitude of K_{op}/K_{max} is constant during the test. However, in 3.5 wt% NaCl solution, since K_{op}/K_{max} varies according to K_{max} increasing, they show the different results with the magnitude of the stress intensity factor. In case of 1.0 Hz, it shows large shift in the low $\triangle K$ region, less than 18 MPa·$m^{1/2}$, but in the region of more than 18 MPa·$m^{1/2}$, degree of data shifting gradually decreases with $\triangle K$ increase. When $\triangle K$ becomes more than 29 MPa·$m^{1/2}$, the data are not shifted because crack closure phenomena do not occur. In cases of 0.1 Hz and 0.01 Hz, the point where data shifting does not occur is predicted in 26 MPa·$m^{1/2}$ and 40 MPa·$m^{1/2}$, respectively.

In Fig. 8, the crack growth rate in 1.0 Hz is larger than that in 0.1 Hz. It is due to combined reaction between the various factors of crack tip blunting, crack branching, wedge effect, hydrogen embrittlement and so on. From the comparison of Fig. 3 and Fig. 8, it is found that, if the effective stress intensity factor range including the crack closure concept is not considered in evaluation of corrosion fatigue characteristics, the crack growth rate by corrosion fatigue can be underestimated in the comparison with actual one.

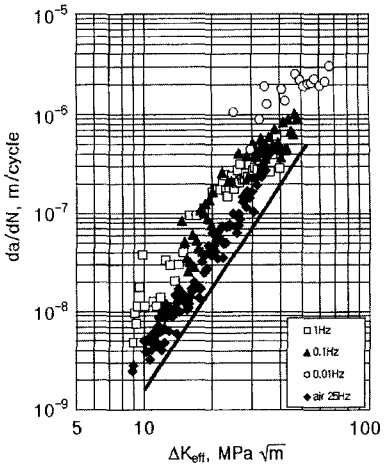

Fig. 8 Representation of corrosion fatigue characteristic curves of Fig. 3 using $\triangle K_{eff}$

5. Conclusion

For reasonable evaluation of the corrosion fatigue characteristics in the weld of A106 Gr B steel pipe, corrosion fatigue tests were conducted in 3.5 wt% NaCl solution at room temperature. And the effects of the various environmental and mechanical factors on crack closer behavior were evaluated using crack closure concept. The results are as follows;

(1) Transition behavior of crack opening was observed in 3.5 wt% NaCl solution at room temperature.

(2) When the loading frequency was 1.0 Hz, the crack opening point was higher than that in air and the low stress intensity factor range. But, it decreased until K_{max} was 20 MPa·$m^{1/2}$.

(3) In the case of 0.1 Hz, the crack opening point decreased continuously.

When K_{max} was 27 MPa·$m^{1/2}$, K_{op} was equal to K_{max}. In case of 0.01 Hz, the similar results to those of 0.1 Hz was qualitatively obtained.

(4) Using the effective stress intensity factor range including the crack closure concept, more consistent corrosion fatigue characteristic curve could be obtained. When the effective stress intensity factor range was not considered in evalua-

tion of corrosion fatigue characteristics, the crack growth rate by corrosion fatigue could be underestimated in the comparison with actual one.

Acknowledgment

The authors are grateful for the support provided by a grant from the Korea Science and Engineering Foundation (KOSEF) and Safety and Structural Integrity Research Center at the Sungkyunkwan University.

References

ASM, 1996, *ASM HANDBOOK*, pp. 644~653.

ASTM, 1981, "Environment Effect on Fatigue Crack Propagation," ASTM Metals Hand Book, Vol. 8, pp. 403~411.

Achilles, R. D. and Bulloch, J. H., 1987, "The Effect of Frequency and Environment on the Fatigue Crack Growth Behavior of SA508 RPV Steel," *IJPVP*, Vol. 30, pp. 171~192.

Bae, D. H. et al., 2002, "Numerical Analysis of Welding Residual Stress Using Heat Source Models for the Multi-Pass Weldment," *KSME International Journal*, Vol. 16, No. 9, pp. 1054~1064.

Chung, S. H. et al., 1989, "Environment Strength Evaluation of Welded Steel Joint in Seawater (Part I: Corrosion Fatigue Crack Growth Behavior for High Cycle)," *KSME International Journal*, Vol. 3, No. 1, pp. 1~5.

Jones, D. A., 1992, "Principles and Prevention of Corrosion," *Prentice Hall*, pp. 364~367.

Lim, J. K. and Kim, Y. J., 1997, "A Study on Properties of Corrosion Fracture Surfaces of GFRP in Synthetic Sea Water," *KSME International Journal*, Vol. 11, No. 3, pp. 249~254.

Murakami, R. et al., 1987, "The Effect of Residual Stress and Corrosion Deposits on Corrosion Fatigue Crack Propagation Rate of Butt Welded Joints in Natural Sea water," *JSME*, Vol. 36, pp. 986~991.

Shi, Y. W. et al., 1990, "Effect of Welding Residual Stresses on Fatigue Crack Growth Behavior in Butt Welds of a Pipeline Steel," *Engineering Fracture Mechanics*, Vol. 36, No. 6, pp. 893~902.

Todd, J. A. et al., 1997, "Crack Closure Effects of Fatigue Crack Growth Thresholds and Remaining Life in an HSLA Steel," *JPVT*, pp. 37~44.